



Bidirectional sun-induced chlorophyll fluorescence emission is influenced by leaf structure and light scattering properties – A bottom-up approach

Shari Van Wittenbergh ^{a,*}, Luis Alonso ^b, Jochem Verrelst ^b, José Moreno ^b, Roeland Samson ^a

^a Laboratory of Environmental and Urban Ecology, Department of Bioscience Engineering, University of Antwerp, Groenenborgerlaan 171, B-2020 Antwerpen, Belgium

^b Image Processing Laboratory, Department of Earth Physics and Thermodynamics, University of Valencia, C/Catedrático José Beltrán 2, E-46980 Paterna, Valencia, Spain



ARTICLE INFO

Article history:

Received 3 July 2014

Received in revised form 10 October 2014

Accepted 12 November 2014

Available online 5 December 2014

Keywords:

Downward fluorescence

Sun-induced Chl fluorescence

Light absorption

Scattering

Reflectance

Transmittance

Light transfer

ABSTRACT

Sun-induced chlorophyll fluorescence (SIF) at leaf level is emitted in both upward and downward directions in the red and far-red part of the spectrum (650–850 nm) when a leaf is illuminated from the upper leaf surface. Hence, total SIF is represented by the sum of the upward and downward emission components. Nevertheless, the downward component of leaf SIF is often not considered despite that downward fluorescence yield ($\downarrow F_Y$) can amount up to 40% of the total fluorescence yield (F_Y_{tot}). Downward SIF is mainly emitted in the far-red, since this part of fluoresced light is highly scattered within leaves, unlike red Chl fluorescence, which is mostly reabsorbed. While total FY can be quite different among distinct species, the relative partitioning between upward and downward fluorescence shows more similarities among different leaf types, especially in the far-red. It is shown that bidirectional SIF emission properties in the far-red can be attributed to the scattering properties of the leaf, whereby an equifacial leaf follows a different trend compared to bifacial leaves. This was done by comparing SIF data with simultaneously measured reflectance, transmittance and fluorescence data by means of the FluoWat leaf clip coupled with an ASD hyperspectral spectroradiometer. These results could further improve Chl fluorescence modeling at leaf level, and help to advance the interpretation of SIF at the canopy level.

© 2014 Elsevier Inc. All rights reserved.

1. Introduction

Sun-induced fluorescence (SIF) emitted by chlorophyll (Chl) pigments is one of the de-excitation mechanisms of plants to cope with an excess in light energy. It competes with photochemical processes, energy transfer and radiationless decay for light excited singlet Chl molecules (Krause & Weis, 1991). Although the direct link with photosynthesis may not be trivial (Meroni et al., 2009), mainly due to the interplay with the other dissipation mechanisms, SIF emitted by vegetation is seen as a meaningful signature of photosynthesis (Porcar-Castell et al., 2014). A major advantage of the SIF signal is that it is a more physiological related signal compared to the reflectance signal, and moreover uniquely originates from vegetation. Whereas the reflectance signal registered by remote sensors reveals rather definitive structural changes in leaves or vegetation canopy covers such as Chl content and leaf area index (Rautiainen et al., 2010; Verrelst, Alonso, Camps-Valls, Delegido, & Moreno, 2012), SIF represents a more fine-tuned physiological signal with a diurnal dynamic (Amoros-Lopez et al., 2008; Flexas et al., 2002).

Although the emitted SIF flux is relatively small compared to the reflected sun radiation (about 2–5% in the near infrared), SIF is a broadband spectrum ranging from 650 nm to 850 nm with two emission peaks in the red around 690 nm and in the far-red around 740 nm (Papageorgiou & Govindjee, 2004). Yet, the red and far-red fluorescence flux that is propagated throughout the leaves is also subjected to internal absorbance and scattering effects, with scattering being divided in reflectance and transmittance. From a bottom-up perspective, scattering and re-absorbance effects continue further at the canopy level, therefore they may play an increasing role when observing vegetation SIF from a remote scale. With the development of hyperspectral sensors with high spectral resolution, the retrieval of SIF has become a novel area of research (Alonso et al., 2007; Gualter et al., 2010; Meroni et al., 2009, 2010), aiming at mapping SIF from a site-specific (Damm et al., 2014; Daumard et al., 2012; Moya, Daumard, Moise, Ounis, & Goulas, 2006; Perez-Priego, Zarco-Tejada, Miller, Sepulcre-Canto, & Fereres, 2005; Zarco-Tejada, Gonzalez-Dugo, & Berni, 2012) towards a global scale (Joiner et al., 2013). Thus far these studies rather emphasized on the development of SIF retrieval methods, thereby taking atmospheric absorption and scattering effects into account (Gualter et al., 2010). A top-down approach is currently pursued by the global SIF mapping community, whereby a meaningful interpretation of the

* Corresponding author. Tel.: +32 3 265 3569; fax: +32 3 265 3225.

E-mail address: Shari.VanWittenbergh@uantwerpen.be (S. Van Wittenbergh).

derived SIF retrievals is searched for, e.g., through seeking for empirical relationships with gross primary production (GPP) (Frankenberg et al., 2011; Guanter et al., 2012, 2014). However, the source of the SIF flux is typically taken for granted and the within-leaf and canopy radiative transfer fluxes have been largely left unstudied. Therefore, in order to close the scaling gap, a bottom-up approach that aims to elucidate the propagation of the SIF flux through a leaf, canopy (re-)absorption and scattering effects and eventually leaving the canopy, is urgently demanded. It is primarily through a better description of (fluoresced) light interaction at the leaf level that will lead to a better interpretation of the remotely retrieved Chl fluorescence signal (Pedrós, Goulas, Jacquemoud, Louis, & Moya, 2010).

SIF is emitted by Chl *a* throughout the different leaf layers, with emission intensity depending on incoming radiation and Chl concentration. Hence, leaves with a higher Chl concentration in the upper leaf layers (typically for bifacial leaves) will produce a higher Chl fluorescence intensity in those layers (Vogelmann & Han, 2000). Internal (re-)absorption of fluoresced light occurs intensively in the red, due to the Chl absorption peak at 681 nm, which has been often demonstrated (Buschmann, 2007; D'Ambrosio, Szabo, & Lichtenhaller, 1992). Far-red SIF (700–750 nm) on the other hand, generally emitted with the highest intensity, is located in the transition zone between highly absorbed red light and highly scattered near-infrared (NIR) light (750–1400 nm). Since within-leaf light scattering will take place in all directions, SIF will be emitted from both leaf sides (Louis, Cerovic, & Moya, 2006). Upward and downward leaf Chl fluorescence spectra have been measured (Louis et al., 2006) and modeled (with FluorMODleaf) based on excitation with laser beams of different wavelengths (Miller et al., 2005). Considering that the shape of the leaf Chl fluorescence spectrum, hence also the red/far-red ratio, depends on the excitation beam's wavelength (Agati, 1998; Louis et al., 2006), laser excited Chl fluorescence probably does not provide the exact fluorescence shape emitted under natural conditions. Sun-induced hyperspectral upward and downward Chl fluorescence, on the other hand, is able to give a more realistic Chl fluorescence shape and better reference for remote sensing purposes (Van Wittenberghe, Alonso, et al., 2014; Van Wittenberghe et al., 2013).

The remote retrieval of Chl fluorescence exploits the Fraunhofer lines, i.e. narrow dark lines of the Sun and Earth's atmospheric transmittance in which irradiance is strongly reduced (Meroni et al., 2009). The most commonly used Fraunhofer features are the O₂-A absorption region at 760.4 nm (Alonso et al., 2007; Guanter et al., 2010; Meroni et al., 2010) or the NIR solar Fraunhofer lines in the range between 740 and 755 nm (Frankenberg et al., 2011; Guanter et al., 2012). Regardless of the pursued approach, currently most of them rely on one retrieval band interval in the second emission peak. Since SIF emission is highly scattered by vegetation in the NIR, description of the signal in both upward and downward directions at leaf level is of relevant importance for the interpretation of the remotely detectable signal. Therefore, the main objective of this study is to investigate the effect of leaf structure, and hence, within-leaf scattering properties onto the bidirectional Chl fluorescence emission, meaning the upward and downward emission components. For this purpose, several species with different leaf structure were examined. Further, the relationship between upward and downward Chl fluorescence is investigated, as well as their contributions to the total leaf Chl fluorescence emission. The paper closes with a discussion on interpreting the upward canopy SIF signal as detected by airborne or spaceborne spectrometers.

2. Materials and methods

2.1. Sun-induced reflectance, transmittance and Chl fluorescence

Sun-induced reflectance (R), transmittance (T) and Chl fluorescence (F) were all measured in situ on leaves attached to their branch by means of the FluoWat leaf clip (Alonso et al., 2007; Van Wittenberghe et al., 2013) connected to a hyperspectral spectroradiometer (FieldSpec,

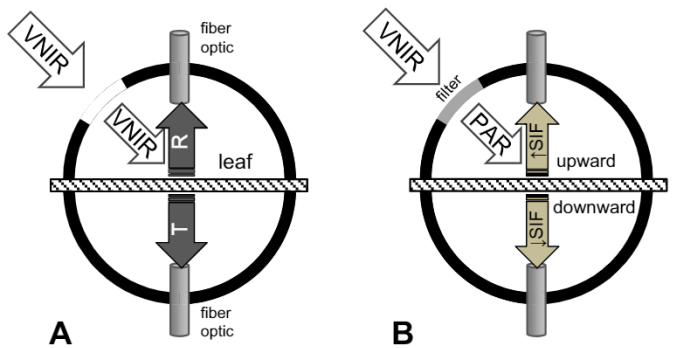


Fig. 1. Scheme of FluoWat leaf clip. Reflectance (R), transmittance (T) and sun-induced fluorescence (SIF) are measured in the visible and near-infrared (VNIR) wavelength range (400–1400 nm) by placing a fiber optic either in upward (\uparrow) or downward (\downarrow) position (A). After placing the short-pass to restrict incoming PAR to visible wavelengths up to 650 nm (B), upward and downward sun-induced fluorescence (\uparrow SIF, \downarrow SIF) are measured (after Van Wittenberghe et al., 2013).

analytical spectral devices (ASDs) Inc., Boulder, USA) on leaf samples from four tree species. The design of the FluoWat leaf clip permits the insertion of the fiber optic of the spectroradiometer in two positions, one upward and one downward with respect to the leaf position (Fig. 1A). In this way, the fiber optic perpendicularly points to the leaf surface from either one of both positions. The leaf with the attached FluoWat leaf clip is then manually positioned so that the incoming solar beam enters the open aperture which is located half-way between the plane of the leaf and the perpendicular positions of the fiber optic probe, at a relative 45° position. Reflectance and transmittance measurements are then obtained using both upward and downward fiber optic insertions of the leaf clip (Fig. 1B). For more details, see Van Wittenberghe et al. (2013). After restricting light entering the aperture with a short-pass filter that cuts off light above 650 nm, upward and downward emitted Chl fluorescence are measured at the upward and downward probe positions, respectively (Fig. 1B). Following this protocol, upward and downward Chl fluorescence are measured with the fiber optic pointing at the same leaf spot were respectively reflectance and transmittance are measured, delivering a combined R-T-F dataset.

Leaves from four tree species, which substantially differ in leaf structure and pigment content, were collected and measured during two field campaigns in the period August 10–31 in 2011 in the city of Valencia in the framework of the BIOHYPE project (Van Wittenberghe, Alonso, et al., 2014; Van Wittenberghe et al., 2013). All sampled trees were sun-exposed and grown at different locations within the urban environment (e.g., street side, park). A first part of the dataset originated from a campaign focusing on trees across the city exposed to either a low or high traffic intensity whereby trees were sampled from the bottom canopy layer (Van Wittenberghe et al., 2013). A second part of the dataset contained leaves taken from trees, whereby three different canopy heights were sampled from three trees per species (Van Wittenberghe, Alonso, et al., 2014). Total sample size of the combined R-T-F spectral dataset of the species European nettle tree (*Celtis australis* L.) ($n = 78$), White mulberry (*Morus alba* L.) ($n = 59$), Canary Island date palm (*Phoenix canariensis* Chabaud) ($n = 66$) and London plane (*Platanus × acerifolia* (Aiton) Willd.) ($n = 59$) was 262 leaves. During both field campaigns, branches from each sampling site were transported to the laboratory with their stems submerged in water prior to spectral analysis. Five healthy leaves of each branch were measured outside the lab under clear sky conditions. After light adaption each leaf was inserted and the leaf clip opening was positioned towards the sun in order to receive direct sun beams on the leaf surface. Hence, the R-T-F dataset is obtained with direct sun beams under a 45° inclination with the leaf surface.

In order to compare the different samples and the different species, Chl fluorescence yield (FY, unitless) was calculated by normalizing the

SIF signal for the absorbed incoming photosynthetic active radiation (APAR) during the measurements. This APAR is calculated by multiplying the integration in the PAR region with the fraction of light absorbed in the PAR region (fAPAR) (Van Wittenberghe et al., 2013). FY is then calculated for the upward (\uparrow FY) and downward (\downarrow FY) Chl fluorescence signals, respectively. Total Chl fluorescence yield (F_{tot} , unitless) of each leaf was calculated as the sum of upward and downward Chl fluorescence yields. The total emitted Chl fluorescence signal (F_{tot} , $\text{W m}^{-2} \text{nm}^{-1} \text{sr}^{-1}$) is also presented in radiance units, to compare the difference between emitted F_{tot} and FY_{tot} among species. The percentage of upward and downward to total Chl fluorescence is calculated, separately for the red and the far-red emission peaks (e.g., $\uparrow F_{687}/F_{687_{\text{tot}}}$, %), characterizing the Chl fluorescence emission curve. To test statistically for differences in bidirectional Chl fluorescence behavior among species, an analysis of variance (ANOVA) and Tukey test ($p = 0.05$) was performed. Data normality was verified with Shapiro-Wilk test. A logarithmic or inverse transformation was used when necessary to comply with normality.

The relationship between bidirectional SIF emission and leaf reflectance and transmittance spectroscopy was investigated. Relationships between bidirectional SIF ratios, defined as the ratio of downward emitted Chl fluorescence at a certain wavelength over the upward Chl fluorescence at the same wavelength (e.g., $\downarrow F_{755}/\uparrow F_{755}$), and reflectance and transmittance ratios at identical wavelengths (e.g., T_{755}/R_{755}) were explored. The same was done for unidirectional SIF ratios (e.g., $\uparrow F_{681}/\uparrow F_{755}$) and R/T ratios (e.g., R_{681}/R_{755}). When overall relationships were weak, quantile regression (QR) (Cade & Noon, 2003; Koenker & Bassett, 1978; Koenker & Hallock, 2001) was used, whereby quantiles with a tau value of 0.025 and 0.975 were plotted together with the median regression ($\tau = 0.50$). For this analysis, we used the package quantreg in the open-source software R 2.13.0 software (www.r-project.org).

2.2. Leaf structure and Chl content

Apart from the leaves collected for the sun-induced R-T-F dataset, an additional collection of 45 leaves for each species was sampled for measurement of leaf layer thickness from images of microscopic cross sections to quantify structural differences among species. Segments of 9 mm diameter were punched out between the main vein and the leaf border and fixed in FAA (formalin-acetic-alcohol, ethanol/acetic acid/formaldehyde (37–40%)/distilled water 10:1:2:7). Next, the leaf tissues were dehydrated by placing them in a sequence of 35–50–65–80–90–100% ethanol solution, followed by a 100% isopropanol solution and an isopropanol/chloroform solution with consecutive ratios of 3:1, 1:1 and 1:3. Each step lasted one day. Then, leaf segments were put in the oven at 40 °C with paraffin and chloroform until the paraffin was melted and the chloroform evaporated, after which they were embedded in paraffin. Finally, cross-sections were made with a rotation microtome (Jung, Heidelberg, Germany), and were colored with safranin and Astra blue. The thickness of the upper epidermis, palisade parenchyma, spongy parenchyma and the lower epidermis was computed from images of the leaf cross sections placed under a digital microscope (Nikon Eclipse 80i, Nikon Instruments Inc., Melville, USA) using ImageJ software (<http://rsbweb.nih.gov/ij/> 3 January 2014) and expressed as a percentage of total leaf thickness. For the monocot *P. canariensis*, of the total mesophyll was calculated instead of palisade and spongy parenchyma.

Total chlorophyll content (Chl *a* + *b*) was quantified on 45 leaves for each species with UV-VIS spectroscopy of pigment extracts using 100% acetone according to (Lichtenthaler & Buschmann, 2001) and expressed in mg m^{-2} . Specific leaf area (SLA) was determined as the ratio of fresh leaf area over dry leaf weight. The latter was determined after drying of leaves at 50–60 °C for five days in a drying oven. Leaf area was determined on the scanned leaf surface.

3. Results and discussion

3.1. Species' difference in leaf structure

Leaf cross sections showed high variation in leaf structure among the four investigated tree species (Fig. 2, Table 1). The three dicot species *C. australis*, *M. alba* and *P. × acerifolia* are characterized by a typical bifacial leaf structure with elongated palisade parenchyma cells at the upper leaf surface and rounded/irregular shaped spongy parenchyma cells inside the lower leaf surface. Nevertheless, some structural differences among those species are observed. First, a difference in cell type and their relative amount was recorded. *C. australis* contains a larger portion of palisade parenchyma, respectively 53%, compared to 39% palisade in both *P. × acerifolia* and *M. alba* (Table 1). On the other hand, *M. alba* leaves develop a multi-layer (up five layers) within the palisade parenchyma which is typical for leaves exposed to large quantities of light or grown in dry habitats (xerophytes). Moreover, samples were observed whereby spongy parenchyma developed as elongated cells so that distinction between palisade and spongy parenchyma cells became diffused (Fig. 2). Second, the species elicited a different amount of intercellular air spaces. A generally more densely packed spongy parenchyma with low amount of intercellular air spaces was noticed in *C. australis* and *M. alba* leaves compared to a high amount in *P. × acerifolia* leaves.

Monocot species, such as the palm *P. canariensis*, consist of leaves which differ structurally strongly from the previous dicot species. Leaves are equifacial, without clear difference in tissue layers between upper and lower leaf surfaces. Further, mesophyll cells are densely packed and round-shaped with low amount of intercellular air spaces. Also, palm leaves are twice as thick as the other species' leaves that were examined.

3.2. Species' difference in within-leaf light scattering

Partly as a result of their differences in leaf layers and cell arrangements, the four species scatter light within a leaf in a different way, both over the visible, the far-red and the NIR spectra (Fig. 3). In the visible (400–700 nm), the monocot *P. canariensis* scatters the highest fraction of light upward (=reflected light), while *P. × acerifolia* scatters the largest downward (=transmitted light) fraction. Since *P. canariensis* does not possess elongated palisade cells which guide light directly into the deeper layers, but instead round-shaped cells which create more interfaces (Fig. 2), more light is reflected from the upper layers compared to the other species. Once passed through the upper cell layers, light is reflected onto the many cell-air and cell-cell interfaces, lengthening the light path, with more chances for interception by pigments. This, combined with the high Chl content of *P. canariensis* (Table 1), results in a relatively low fraction of the transmitted or downward scattered light in the visible or PAR region (Fig. 3). In contrast, all three dicots have thinner leaves, with more intercellular air spaces and lower Chl content (especially *P. × acerifolia*), resulting in proportionally more downward scattered light which has not been intercepted by Chl (Fig. 3).

At wavelengths above 700 nm, outside the absorption region for pigments where light is greatly scattered, clear differences among the species can also be observed. These differences are more pronounced for the downward scattered or transmitted light as compared to the upward scattered or reflected light (Fig. 3). This is no surprise, since leaf structure has interacted to a greater extent with the light that passed through the whole leaf section compared to light that is mostly reflected from the upper leaf layers. Without the effect of light absorption by pigments in VIS wavelengths, the structural differences among the species are more pronounced. It is known that the NIR and the SWIR regions contain more information on leaf structure compared to the VIS (Curran, Dungan, & Peterson, 2001; Thenkabail, Enclona, Ashton, & Van der Meer, 2004; Van Wittenberghe, Verrelst, et al., 2014).

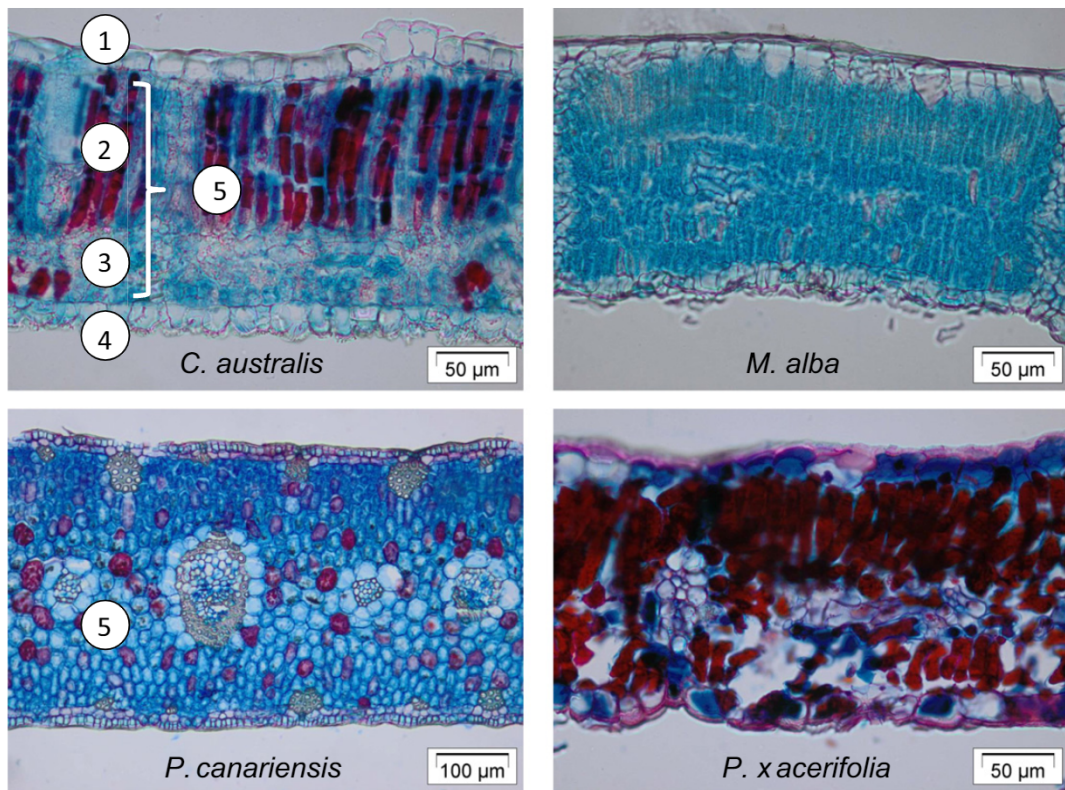


Fig. 2. Leaf cross sections of the four species showing the upper epidermis (1), palisade parenchyma (2), spongy parenchyma (3), lower epidermis (4) and mesophyll (5) layer; note the different scale in the case of the monocot, *P. canariensis*.

P. canariensis clearly transmits the lowest fraction of NIR, while *P. x acerifolia* with the lowest Chl and SLA, transmits the highest fraction. *M. alba* and *C. australis* show similar behavior concerning bidirectional light scattering, with comparable fractions of far-red (700–750 nm) and NIR (>750 nm) reflectance and transmittance, illustrating a similar effect of leaf structure onto the light scattering process. Although *M. alba* and *C. australis* do not show similar amounts of palisade and spongy parenchyma (Table 1), the low amount of intercellular air spaces and similar leaf thickness probably caused similar light scattering behavior in both species.

3.3. Total Chl fluorescence yield and ratios

The total amount of absolute radiated SIF (F_{tot}) varies little among for the three dicot species but total was lowest for the monocot species,

Table 1

Leaf structure description of the four species showing total leaf thickness (μm) and the percentage of the different leaf layers (mean \pm standard deviation).

Species	<i>P. x acerifolia</i>	<i>M. alba</i>	<i>C. australis</i>	<i>P. canariensis</i>
Leaf type	Bifacial	Bifacial	Bifacial	Equifacial
Total thickness (μm)	185 \pm 21	186 \pm 35	226 \pm 61	396 \pm 36
Palisade layers (#)	1–2	1–5	1–3	0
Amount of intercellular air spaces	High	Low	Low	Low
Upper epidermis (%)	11 \pm 2	12 \pm 3	10 \pm 3	6 \pm 2
Mesophyll (%)	–	–	–	89 \pm 3
Palisade parenchyma (%)	39 \pm 5	39 \pm 8	53 \pm 7	–
Spongy parenchyma (%)	38 \pm 5	41 \pm 8	27 \pm 4	–
Lower epidermis (%)	11 \pm 2	8 \pm 2	9 \pm 2	5 \pm 1
Specific leaf area ($\text{cm}^2 \text{g}^{-1}$)	49.2 \pm 7.6	84.9 \pm 20.8	71.2 \pm 19.9	112.4 \pm 19.0
Chl content (mg m^{-2})	404 \pm 95	753 \pm 272	888 \pm 142	1244 \pm 279

P. canariensis (Table 2). The fluorescence yields ($FY_{\text{tot}}, \uparrow FY, \downarrow FY$), i.e., the percentage of energy that is emitted as SIF based on the energy that is absorbed by the leaf, varies somewhat more among the dicot species, which exceed the FYs for the monocot. Total FY is highest for *M. alba*, followed by *C. australis* and *P. x acerifolia*, and then by *P. canariensis* (Fig. 4). However, it has to be noticed that having similar total or upward FY, as in case of *C. australis* and *P. x acerifolia* (Table 2), does not imply similar Chl fluorescence shapes as can be seen from the emission spectra plotted in Fig. 4. Hence, FY on its own does not hold all the information. The red/far-red peak ratios indicate better Chl fluorescence

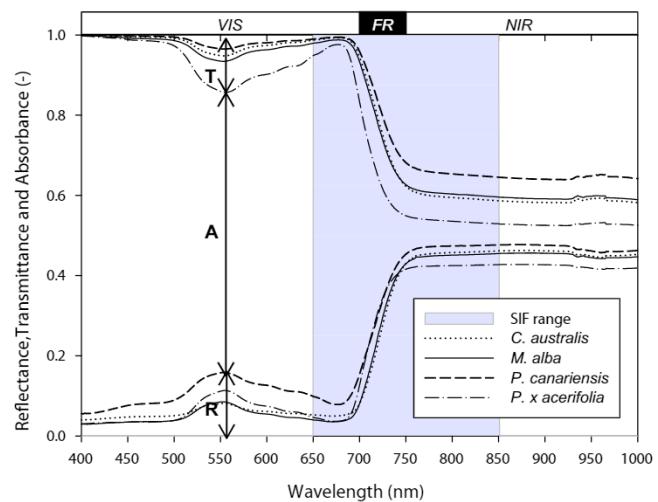


Fig. 3. Average reflectance (R), transmittance (T) and absorbance (A) for the four species in the visible (VIS), far-red (FR) and part of the near-infrared (NIR); sun-induced fluorescence (SIF) is emitted in the indicated shaded spectral area.

Table 2

Tukey test after analysis of variance (ANOVA) for the bidirectional Chl fluorescence behavior among the four species; different small letters indicate significant species differences ($p < 0.05$).

Species	<i>P. × acerifolia</i>	<i>M. alba</i>	<i>C. australis</i>	<i>P. canariensis</i>
F_{tot} ($\text{W m}^{-2} \text{nm}^{-1} \text{sr}^{-1}$)	$0.120 \pm 0.050\text{a}$	$0.117 \pm 0.046\text{a}$	$0.101 \pm 0.032\text{a}$	$0.068 \pm 0.029\text{b}$
FY_{tot} (%)	$0.269 \pm 0.086\text{b}$	$0.307 \pm 0.068\text{a}$	$0.257 \pm 0.062\text{b}$	$0.194 \pm 0.051\text{c}$
$\uparrow FY$ (%)	$0.162 \pm 0.054\text{b}$	$0.204 \pm 0.051\text{a}$	$0.170 \pm 0.047\text{b}$	$0.130 \pm 0.037\text{c}$
$\downarrow FY$ (%)	$0.107 \pm 0.034\text{a}$	$0.103 \pm 0.023\text{a}$	$0.087 \pm 0.019\text{b}$	$0.065 \pm 0.016\text{c}$
$\uparrow FY/FY_{\text{tot}}$ (%)	$60.0 \pm 3.1\text{b}$	$66.2 \pm 4.8\text{a}$	$65.9 \pm 3.7\text{a}$	$66.5 \pm 4.0\text{a}$
$\downarrow FY/FY_{\text{tot}}$ (%)	$40.0 \pm 3.1\text{a}$	$33.8 \pm 4.8\text{b}$	$34.1 \pm 3.7\text{b}$	$33.5 \pm 4.0\text{b}$
$\uparrow F687/F687_{\text{tot}}$ (%)	$65.1 \pm 5.2\text{c}$	$81.8 \pm 6.1\text{b}$	$84.3 \pm 4.6\text{b}$	$87.9 \pm 7.6\text{a}$
$\uparrow F741/F741_{\text{tot}}$ (%)	$58.6 \pm 2.6\text{b}$	$61.7 \pm 4.3\text{a}$	$61.1 \pm 3.0\text{a}$	$59.0 \pm 3.4\text{b}$
$\uparrow F687/\uparrow F741$	$0.93 \pm 0.33\text{a}$	$0.65 \pm 0.08\text{b}$	$0.50 \pm 0.07\text{c}$	$0.75 \pm 0.23\text{b}$
$\downarrow F687/\downarrow F741$	$0.76 \pm 0.41\text{a}$	$0.24 \pm 0.10\text{b}$	$0.15 \pm 0.04\text{c}$	$0.18 \pm 0.20\text{bc}$
$F687_{\text{tot}}/F741_{\text{tot}}$	$0.86 \pm 0.36\text{a}$	$0.49 \pm 0.09\text{b}$	$0.37 \pm 0.05\text{c}$	$0.51 \pm 0.20\text{b}$

shape differences among species and show statistical differences among the species (Table 2).

The percentage of total SIF emission emitted upward ($\uparrow FY/FY_{\text{tot}}$) is, however, more constant among the species at 60% to 67% leaving ~40% of FY_{tot} to be emitted downward. A considerable amount of Chl F emission is thus not taken into account when measurements are carried out unidirectionally from above the leaves' upper surfaces. There is a large difference in the fraction of red vs. far-red emitted upward and downward. The fraction of the total red SIF that is emitted upward ($\uparrow F687/F687_{\text{tot}}$) ranges between 65.1% (*P. × acerifolia*) and 87.9% (*P. canariensis*). However, the fraction of the total far-red SIF emitted upward ($\uparrow F741/F741_{\text{tot}}$) is more similar (~61%) among the different species.

3.4. Relationship between upward, downward and total Chl fluorescence

The relationship between upward and downward SIF was investigated for all species. Downward emitted FY is linearly positive related to the upward emitted FY (Fig. 5), with the goodness-of-fit being highest for *P. × acerifolia* ($R^2 = 0.86$) which has the lowest Chl content.

The downward red/far-red peak ratio ($\downarrow F687/\downarrow F741$) is found overall to be lower compared to the upward red/far-red peak ratio ($\uparrow F687/\uparrow F741$) (Table 2, Fig. 6A), due to re-absorption of red emitted fluorescence along the optical path through the leaf, which reduces the $\downarrow F687$ SIF intensity. Only in a few cases of *P. × acerifolia* downward red/far-red peak ratio exceeded its upward counterpart, indicating that re-absorption with respect to emission of red SIF is lower at the downside of the leaf. High downward peak ratios were in previous research found for *P. × acerifolia* leaves exposed to a high traffic pollution (Van Wittenbergh et al., 2013). This could mean that Chls located at deeper leaf layers performed a lower re-absorption capacity compared to Chls located at upper leaf layers. Since stomata, only present at the lower leaf side of *P. × acerifolia*, act as the interface between leaf and atmosphere, gaseous pollutants primarily enter the leaf by diffusion from this stomatal leaf side. Therefore it seems evident that the first place of less-functioning Chl due to air pollutants happens at the leaf interior's lower part.

With a generally lower downward peak ratio, the peak ratio of total emitted fluorescence ($F687_{\text{tot}}/F741_{\text{tot}}$) will evidently also become smaller than the upward peak ratio $\uparrow F687/\uparrow F741$ (Figs. 4, 6B).

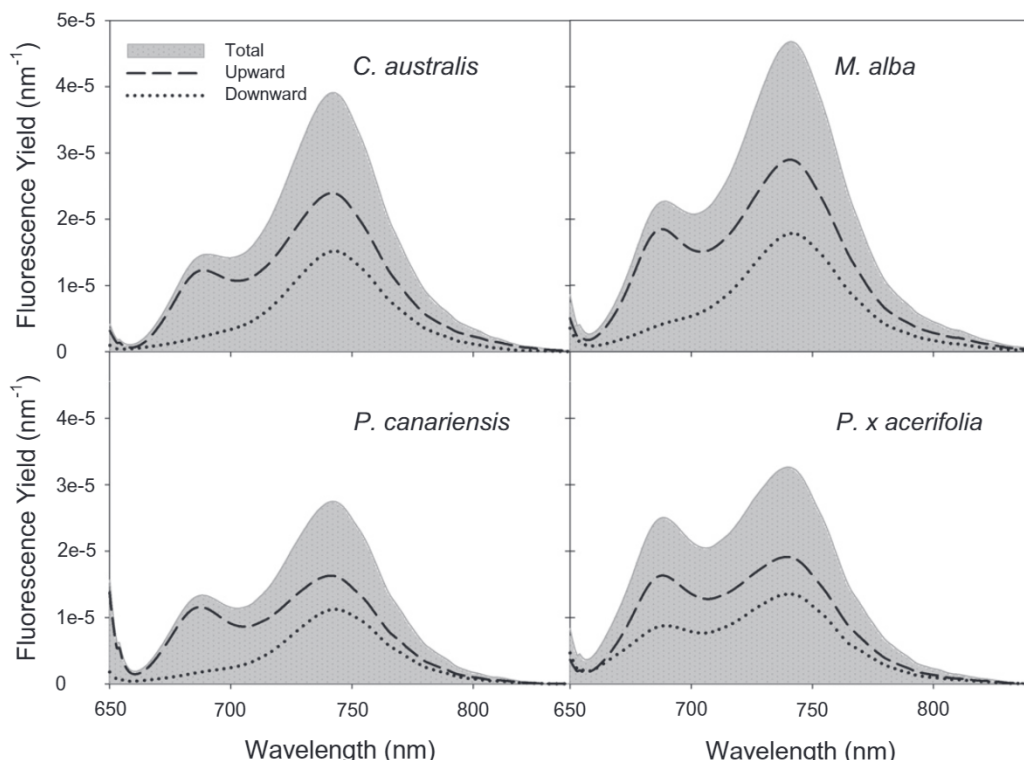


Fig. 4. Typical individual leaf level total (shaded area) as well as upward (dashed curves) and downward (dotted curves) Chl fluorescence yields for the four species.

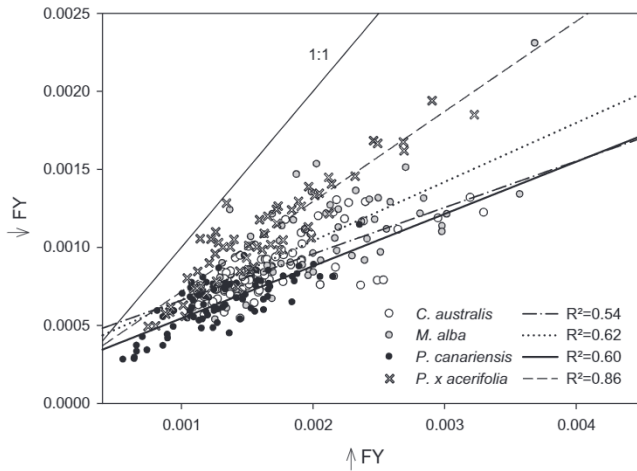


Fig. 5. Linear regression between upward Chl fluorescence yield (\uparrow FY) and downward Chl fluorescence yield (\downarrow FY) with the coefficient of determination (R^2) for the four species.

Additionally, when relating the upward and total red/far-red peak ratios a linear match is found for all species. A good linear match between both peak ratios is found when analyzing this relationship for each species separately (Fig. 7). This offers the potential to calculate speciewise $F_{687\text{tot}}/F_{741\text{tot}}$ when only $\uparrow F_{687}/\uparrow F_{741}$ is known.

3.5. Re-absorption and scattering effects onto bidirectional Chl F emission

By calculating the $\downarrow F/\uparrow F$ ratio over the whole fluorescence range for the different species, the re-absorption versus scattering effect is better illustrated (Fig. 8). Low values for $\downarrow F/\uparrow F$ indicate high reabsorption. A minimum at 680–684 nm appears for all species, corresponding to the red absorption maxima of Chl pigments at these wavelengths. The difference among species is clearly seen here, with *P. canariensis* showing the lowest value at this minimum, and *P. x acerifolia* showing the highest value. From 740 nm onward, the influence of re-absorption has disappeared, resulting that at these wavelengths $\downarrow F/\uparrow F$ is mostly determined by (i) the channeling and scattering of far-red light within the leaf section, and (ii) the amount of Chl F that is emitted in the lower leaf layers. This latter component seems to be more significant for *P. canariensis*, as this leaf type does not transmit far-red light as easily as the other species (Fig. 3). Therefore, the higher $\downarrow F/\uparrow F$ level in relation to *M. alba* and *C. australis* is rather explained by a more equally distributed Chl content throughout the mesophyll layer, causing relatively

higher Chl F emission in deeper leaf layers. From a deep “re-absorption” valley, the curve shows a steep increase to a high $\downarrow F/\uparrow F$ at 740 nm. It illustrates re-absorption close to the 680 maximum taking place until the deeper leaf layers, while Chl F emission is still emitted from these layers in case of the thick palm leaves.

C. australis and *M. alba* show a similar $\downarrow F/\uparrow F$ curve. It reflects their similar absorption-scattering profile that was already shown in Fig. 3, indicating a comparable effect of their similar pigment content and leaf structure onto the light scattering at the different wavelengths. To illustrate better the connection between light scattering behavior and SIF emission, fluorescence data was compared with simultaneously measured reflectance and transmittance data. We concentrated on wavelengths where the absorption effect (at 681 nm, corresponding with the absorption maximum in the red) and scattering effect (at 755 nm, outside the re-absorption influence) were high.

We found that $\downarrow F_{681}/\uparrow F_{681}$ is related to the inverse of transmittance at the same wavelength ($1/T_{681}$) according an exponential decay function (Fig. 9A). As most SIF is assumed to originate from the upper leaf layers due to higher light intensity and higher Chl content, downward SIF will be highly influenced by the light transmittance properties of the leaf (rather than reflectance properties). The fraction of $\downarrow F_{681}/\uparrow F_{681}$ represents the part of SIF that is emitted downward compared to the part emitted upward, which assumingly comes mostly from the upper leaf layers. Hence, the fluorescence fraction that traveled from the upper to the lower leaf side will endure the same “resistance” as non-fluoresced light from the same wavelength. This can be best defined by the transmittance at the same wavelength. Moreover, by taking the inverse T_{681} , the ‘extinction effect’ due to re-absorption is better described.

At 755 nm, a wavelength where no re-absorption effect is noticed anymore, and at the same time close to the O_2-A absorption band, the bidirectional ratio ($\downarrow F_{755}/\uparrow F_{755}$) was compared with the respective T_{755}/R_{755} ratio (Fig. 9B). Both parameters showed a positive linear trend. A linear regression was plotted for the equifacial leaf and the group of bifacial leaves separately. The latter had a higher goodness-of-fit compared to the first. Of course, a perfect linear relationship between $\downarrow F_{755}/\uparrow F_{755}$ and T_{755}/R_{755} cannot be expected due to one main reason. Transmitted and reflected light originates from the sun irradiance falling onto the leaf surface, while fluoresced light originates from inside the leaf at different leaf layers. Hence, different within-leaf light paths and scattering interactions will result in a different partitioning between upward and downward scattered light compared to light which is either reflected or transmitted. Nevertheless, the processes of within-leaf light scattering will be mostly characterized by its leaf structure, resulting in a positive trend between both ratios. For

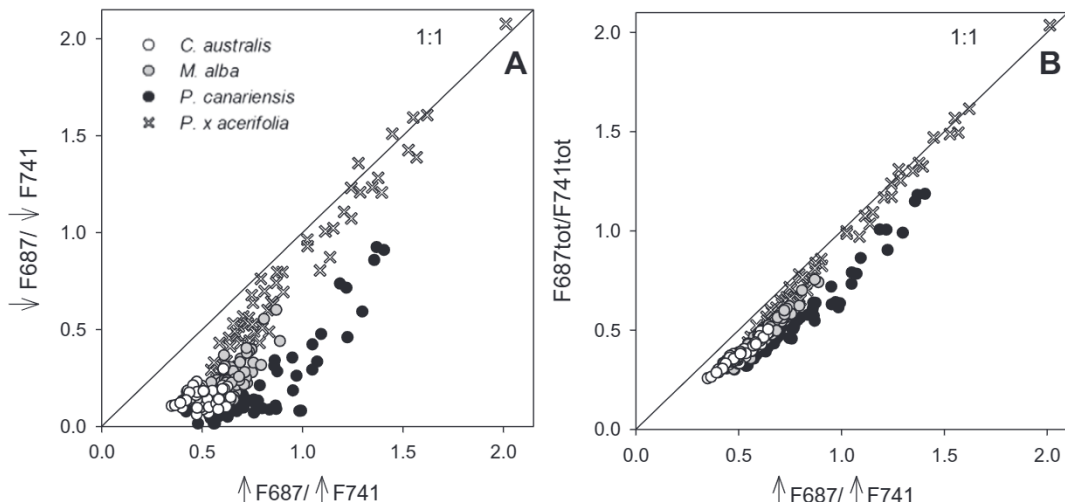


Fig. 6. Comparison of the red/far-red peak ratios for upward (\uparrow) and downward (\downarrow) Chl fluorescence emissions (A) and upward and total Chl fluorescence emissions (B).

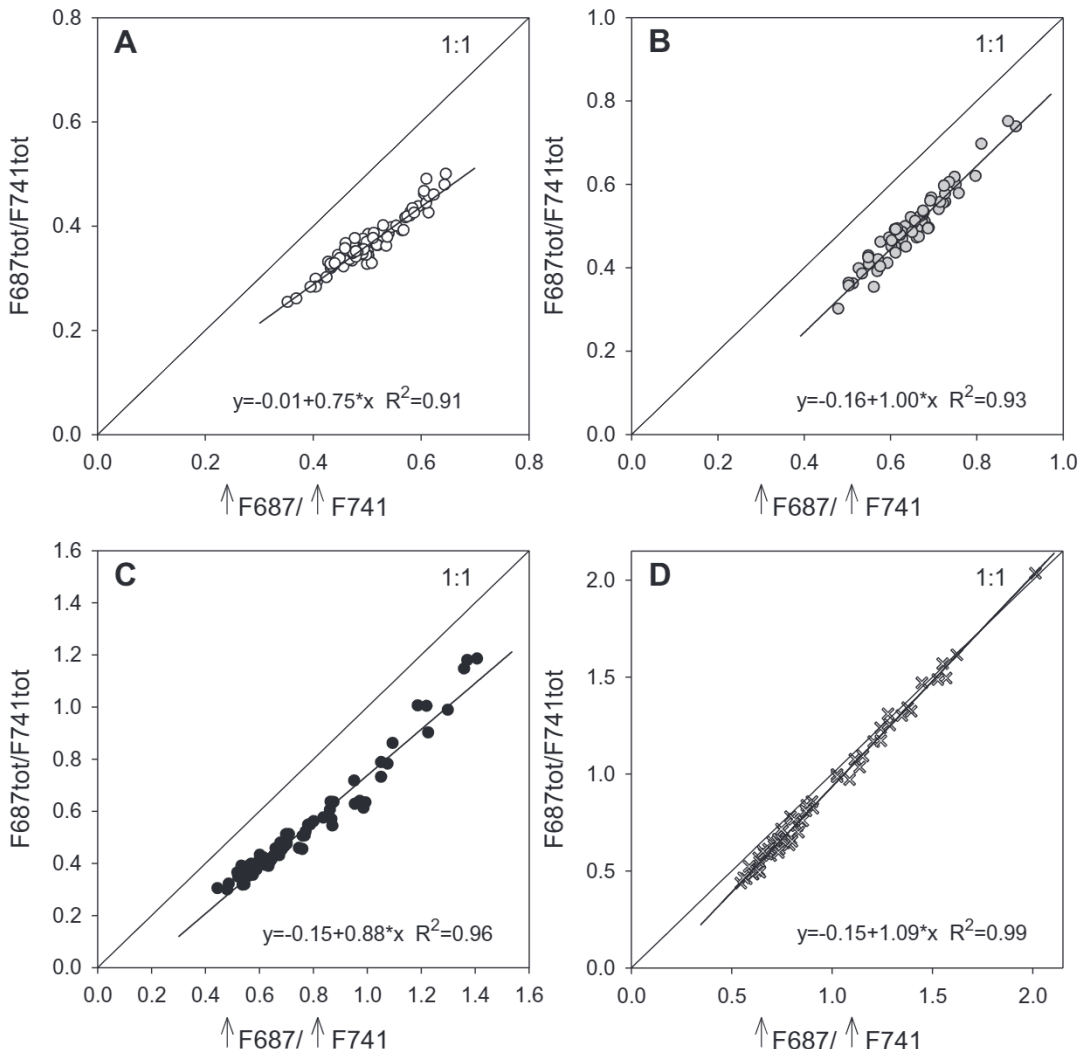


Fig. 7. Linear relationship between upward (\uparrow) and total (tot) red/far-red peak ratios for *C. australis* (A), *M. alba* (B), *P. canariensis* (C) and *P. × acerifolia* (D). Scales vary for each panel, A–D.

describing a general variation trend, quantile regression (QR) was used, showing a wider variation the higher both parameters.

The mechanism of downward scattering is favored in leaves with a typical bifacial leaf structure containing a considerable amount of air

spaces. *P. × acerifolia*, for example, has the highest T755/R755 ratio. *P. canariensis*, on the other hand, has rather low T755/R755 values. For the same T755/R755 ratio, the palm tree has a higher $\downarrow F755/\uparrow F755$ ratio compared to the bifacial leaf types, which might indicate that relatively more Chl fluorescence is emitted from the lower leaf layers.

When evaluating the effect of SLA on T755/R755 on one hand, and on $\downarrow F755/\uparrow F755$ on the other hand, the importance of leaf structure on $\downarrow F755/\uparrow F755$ is better illustrated (Fig. 10). Specific leaf area, which represents the area per dry matter, is low for leaves with a high amount of dry matter per leaf area, and high for leaves with less amount of dry matter per leaf area. The parameter, however, does not contain information on how this dry matter is structured. For sun light arriving onto the upper leaf surface, there is a significant effect of SLA on T755/R755 (Fig. 10A), meaning that the amount of dry matter is indicative for the light passing through the whole leaf section (T755). For $\downarrow F755/\uparrow F755$, this is not the case (Fig. 10B), illustrating that fluorescence emitted from the leaf interior will be also influenced by other factors such as location of emission (pigments) and leaf structure.

Further, upward and downward F681/F755 ratios were compared with R681/R755 and T681/T755 respectively (Fig. 11). The upward SIF ratio ($\uparrow F681/\uparrow F755$) compared with upward scattering ratio (R681/R755) shows a positive trend, mostly directed by *P. canariensis* data (Fig. 11A). An explanation for this might be that light at 681 nm is scattered more from the upper layers for this equifacial leaf type, enhancing the relationship with fluoresced (also scattered) light produced

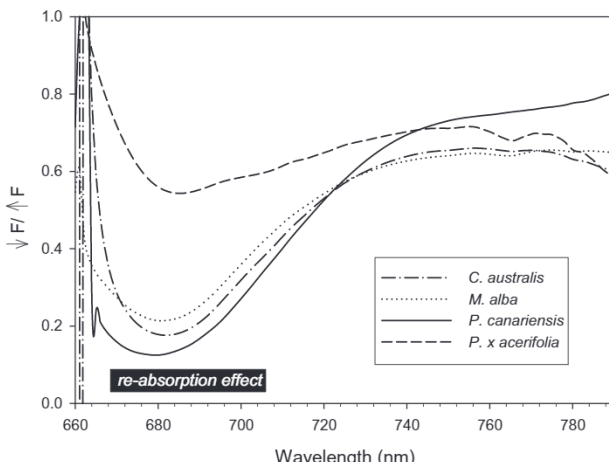


Fig. 8. Downward to upward ratio for the Chl fluorescence spectrum ($\downarrow F/\uparrow F$) for the four species.

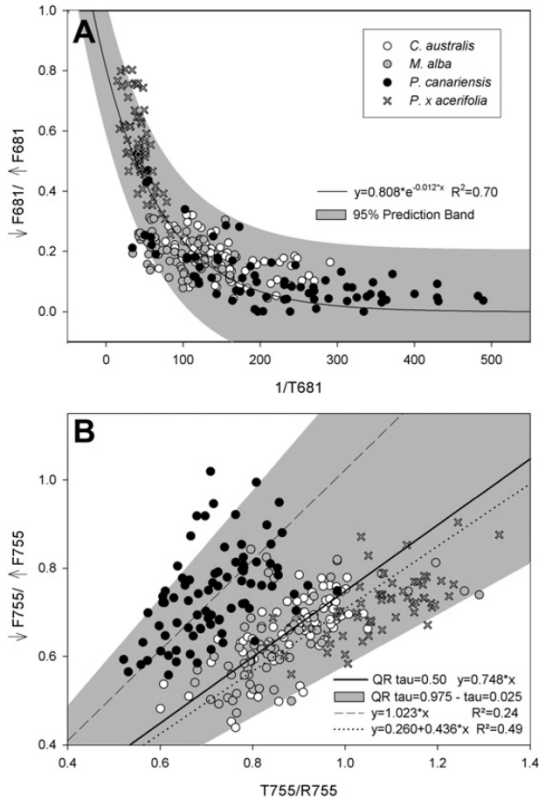


Fig. 9. Exponential decay function with 95% prediction band between the bidirectional Chl fluorescence emission ratio in the red ($\downarrow F681/\uparrow F681$) and the inverse of transmittance in the red ($1/T681$) (panel A) and quantile regression (QR) analysis between the bidirectional Chl fluorescence emission ratio in the far-red ($\downarrow F755/\uparrow F755$) and the bidirectional scattering ratio in the far-red ($T755/R755$) (panel B); linear regression equations are given for *P. canariensis* data (dashed line) and the group of *C. australis*, *M. alba* and *P. x acerifolia* (dotted line).

in the upper leaf layers. Gitelson, Buschmann, and Lichtenthaler (1998) demonstrated a linear trend between upward $F685/F735$ and $R685/R735$ for two bifacial leaf types, arguing the main influence of Chl content. It is indeed the major influence of leaf pigments' absorption in the red causing this linear trend. When including more leaf types, more scatter rises on this linear trend. The downward SIF ratio ($\downarrow F681/\uparrow F755$) shows a better relationship with the according downward scattering ratio (both parameters are presented as their inverse for a better fitted relationship), which is explained by a larger influence of leaf spectroscopy, hence absorbance by pigments, onto the downward SIF signal.

3.6. Consequences for remote signal of Chl fluorescence

It must be emphasized that observed within-leaf scattering and absorption processes propagate further throughout the canopy. Within a canopy, multiple scattering and absorption effects between different layers of foliage take place. Additionally, the orientation of the leaves, and hence the angle of light incidence, will play a role in SIF emission. Considering our dataset was obtained by illuminating leaves with direct solar illumination under an angle of 45° and measured in zenith position, it does not include multi-angle spectral outcomes of fluorescence emission. A few studies comparing leaf level with canopy level Chl fluorescence report a decrease in (upward) red/far-red peak ratio from leaf to canopy measurements, up to a factor two (Fournier et al., 2012; Moya et al., 2006). As general cause, the authors put forward the re-absorption effect of red emitted SIF as predominating factor (Daumard et al., 2012; Fournier et al., 2012). Indeed, red emitted SIF will be highly re-absorbed within the canopy. Red SIF that is emitted from the lower canopy region

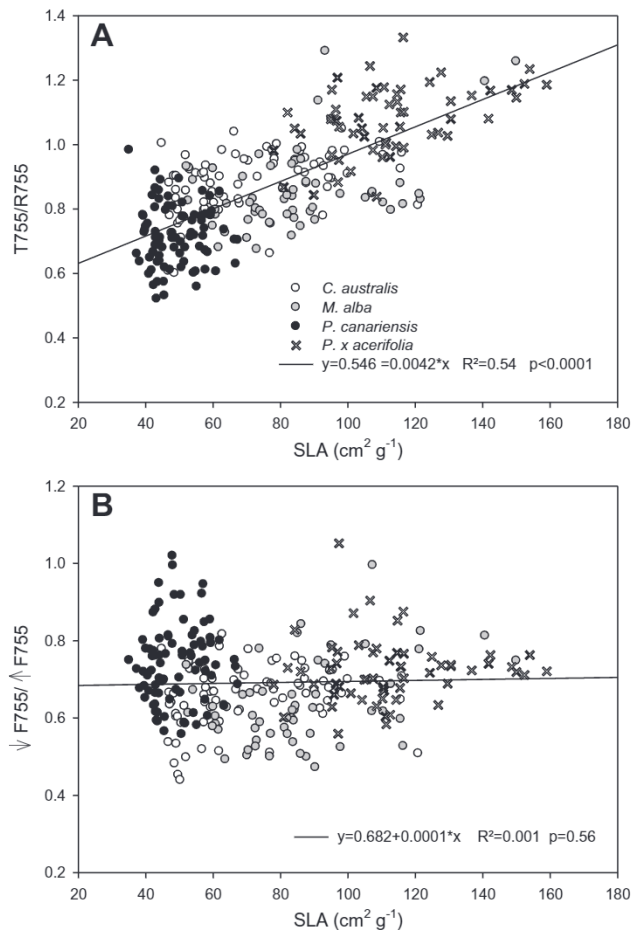


Fig. 10. Linear effect of specific leaf area (SLA) on $T755/R755$ (panel A) and on $\downarrow F755/\uparrow F755$ (panel B).

will have high chances of interception by Chl pigments located in the above canopy region. However, additionally, the far-red part of Chl fluorescence emission will be highly scattered by vegetation (Fig. 3). Therefore, we hypothesize that both systematical multiple re-absorption and scattering effects will cause decreasing of the red/far-red peak ratio at canopy level as compared to the leaf level.

Hence, a lowering in red/far-red peak ratio from leaf to canopy level will be driven by two effects. On one hand re-absorption of the red Chl fluorescence will take place, both at the leaf and canopy scale. On the other hand, far-red Chl fluorescence, which is highly scattered in both directions at leaf level, will be also further scattered by the surrounding leaves and increase its relative contribution to the remotely detected far-red Chl fluorescence from vegetation (Fig. 12). The influence of downward far-red Chl fluorescence from the top canopy layer that will be scattered upwards by the foliage just below, will hereby probably add significantly to the remote signal. As light intensity will decrease with canopy depth, the SIF signal intensity will decrease comparably, since fluorescence emission intensity is mainly driven by PAR intensity (Amoros-Lopez et al., 2008). This implies that the remote SIF signal mainly originates from the SIF fluxes originating from the top canopy layer. Thus, canopy structure will define not only the amount of light penetrating through the upper layers, but also the scattering effects taking place here. Vegetation structure would therefore, as suggested already by several authors (Fournier et al., 2012; Miller et al., 2005), impose a considerable impact onto the canopy Chl fluorescence detected from a remote platform.

Given that the second peak of the SIF emission in the far-red to NIR spectral window (710–850 nm) is strongly influenced by leaf and canopy structure it bears the consequence that for SIF retrievals relying on

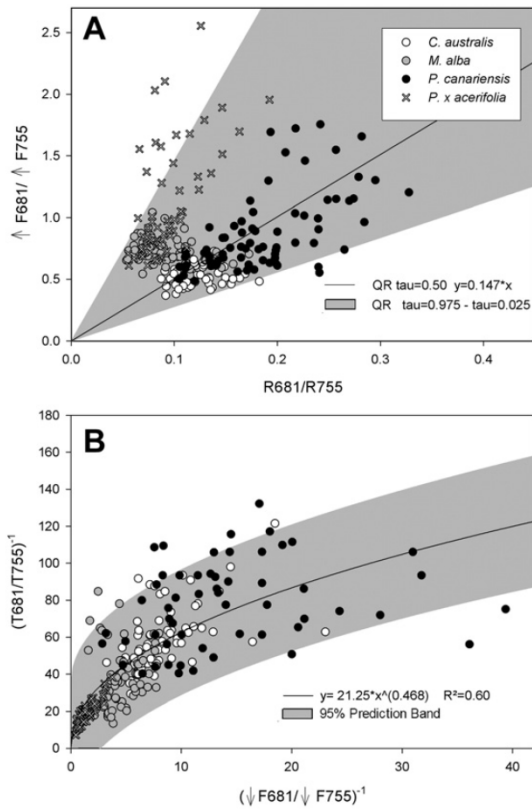


Fig. 11. Quantile regression (QR) analysis between the upward red/far-red Chl fluorescence ratio ($\uparrow F681/\uparrow F755$) and the red/far-red reflectance ratio ($R681/R755$) (panel A), and a power function and corresponding 95% prediction band plotted between the downward inverse red/far-red Chl fluorescence peak ratio and the corresponding transmittance ratio (panel B).

NIR Fraunhofer lines (Frankenberg et al., 2011; Guanter et al., 2012; Joiner et al., 2011) spatial variations in vegetation structure likely influence spatial variations of SIF observations. Effectively, by exploiting these Fraunhofer lines it has been reported that more complex canopies such as forests lead to lower SIF retrievals as opposed to structurally simpler neighboring canopies such as croplands (Guanter et al., 2014). Nevertheless, there is no experimental evidence that tree leaves emit a substantial lower SIF as opposed to grass or crop leaves (Amoros-Lopez et al., 2008). Moreover, forests typically have a considerably denser leaf package (i.e., higher LAI) and tree leaves can reach higher chlorophyll content than croplands (Delegido et al., 2014; Garrigues et al., 2008; Morissette et al., 2006). A pronounced SIF emission into space would therefore be expected. Why this is not observed by current SIF retrieval approaches can be largely explained by the enhanced multiple scattering effects due to a more complex canopy. Forest canopies can be more than a factor 10 times taller than croplands with complex architecture, clumping and gaps (especially coniferous trees; Rautiainen & Stenberg, 2005). Hence forests allow substantially more probability for light to penetrate, absorb and scatter, thereby imposing far-red SIF emissions to scatter throughout the canopy in all directions. At the same time, large parts of trees can be shaded as a function of tree density and architecture (e.g., coniferous trees) leading to a generally weaker signal. Consequently, leaf and canopy structural effects not only suppress the absorption effect but may become dominant determinant of the radiative transfer systems' behavior in the far-red and NIR (Knyazikhin et al., 2013). Consequently, it is hypothesized that tall, heterogeneous canopies lead to an overall more hemispherically scattered SIF flux in the far-red and NIR, and therefore relatively lower at-sensor SIF intensity as opposed to more homogeneous and structurally simpler canopies.

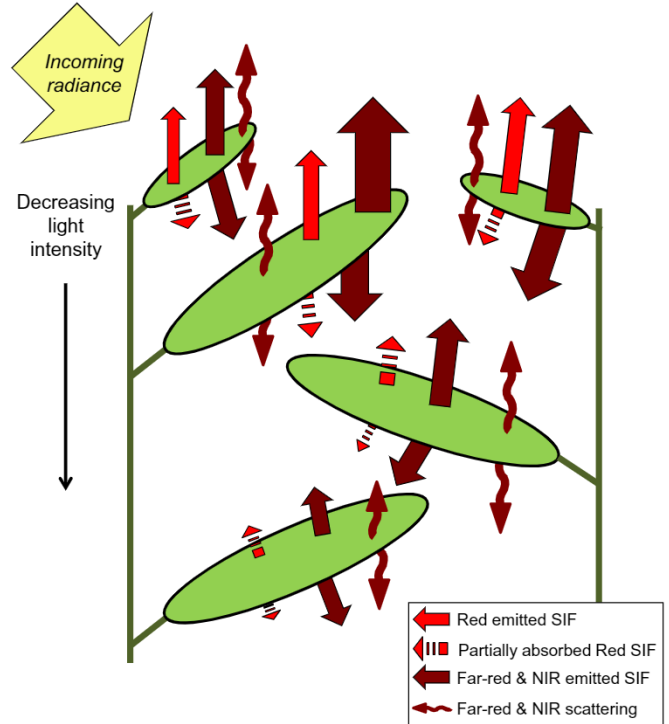


Fig. 12. A simplified scheme of sun-induced fluorescence (SIF) emissions and interactions at canopy level decreasing with decreasing light intensity; Red fluorescence emission is merely re-absorbed, while far-red and near-infrared (NIR) fluorescence emission is scattered up- and downward.

An explicit quantification of canopy structural parameters (e.g., leaf area index, leaf angle distribution) through reflectance data will, therefore, be necessary for further interpretation of the SIF signal obtained via remote sensing. The importance of leaf and canopy structure thus far has been largely overlooked by recent global mapping approaches and subsequent interpretations. This can be especially problematic with low-resolution sensors with a pixel size (e.g., > 7000 m) that spans a surface mostly beyond the size of a homogeneous, structurally simple canopy (with regional exceptions, e.g. the US Corn Belt). Although Guanter et al. (2012) earlier emphasized the role of structural effects by demonstrating that relationships between SIF and photosynthetic activity (GPP) depend on the biome vegetation type. The ignorance of structural effects on radiative transfer properties within a pixel makes that current interpretation of global at-sensor SIF retrievals towards GPP remain largely speculative.

Having appraised the role of leaf and canopy structural effects, it requires more refined strategies to enable disentangling the information content related to photosynthetic activity from vegetation structure. Two strategies are currently on the table: (1) the exploitation of the full SIF emission, i.e. both the first and second emission peak; and (2) making use of jointly derived biophysical variable to adjust for structural effects. As described above, the first emission peak in the red is less affected by multiple scattering effects throughout the canopy. While this peak is generally lower at sensor due to reabsorption by chlorophyll pigments, it implies that the SIF photons reaching the sensor is predominantly coming from the canopy top-layer but also have undergone less multiple scattering effects, therefore providing a more direct (i.e. less affected by multiple scattering) link to photosynthetic activity. At the same time, additional estimation of biophysical variables that provides critical information on vegetation structure (e.g., leaf area index, clumping index) and biochemical constituents (e.g., chlorophyll content) are foreseen to identify and adjust SIF–photosynthesis relationships for structural effects (Verrelst, Alonso, Rivera, Moreno, & Camps-Valls, 2013).

None of the global atmospheric spectrometers currently operative in space (GOSAT, SCIAMACHY, GOME-2, OCO-2) or being planned in near future (e.g., GOSAT-2, Sentinels 4–5) are optimized to cope with either one of these two strategies at a high spatial resolution (e.g., pixel size of <1000 m). It demands the urgent necessity for a dedicated mission. As a candidate of becoming the 8th Earth Explorer mission, ESA has recently initiated a mission that specifically aims to exploit both strategies to the fullest, being FLEX (Fluorescence Explorer). Contrary to current and proposed atmospheric spectrometers, FLEX will be equipped with an imaging spectrometer (FLORIS) specifically designed to reconstruct the full broadband SIF signal, i.e. including both emission peaks ranging from 677 to 780 nm at 0.3 nm, at a continuous spatial resolution of 300 m, providing high resolution and a global bi-weekly repeat coverage (Kraft et al., 2013; Moreno et al., 2006). At the same time FLEX will also cover the PRI region (500–600 nm) and the chlorophyll absorption region (600–677 nm) and is planned to fly in tandem with ESA Sentinel-3 in order to deliver other critical variables to facilitate the signal interpretation and adjustment (e.g., canopy temperature, fAPAR, LAI, chlorophyll content) (Kraft et al., 2013). Only such unprecedented and unique spatially continuous dataset will prompt an unbiased monitoring of the globe's vegetation vitality and be able to unravel the physiological relationships with GPP and photosynthetic carbon uptake.

4. Conclusions

The total SIF flux combining upward and downward emissions by the leaf has a lower red/far-red peak ratio ($F_{687\text{tot}}/F_{741\text{tot}}$) compared to the peak ratio of just the upward emitted Chl fluorescence ($\uparrow F_{687}/\uparrow F_{741}$). This is due to a considerable amount of far-red Chl fluorescence that is emitted by the downward side of the leaf (up to 40% of F_{tot}), which is not taken into account when measuring only from the upper leaf surface. However, it is shown that $F_{687\text{tot}}/F_{741\text{tot}}$ can be estimated from $\uparrow F_{687}/\uparrow F_{741}$ with good accuracy at species level.

The partitioning of bidirectional Chl fluorescence into an upward component and downward component is influenced by scattering and absorption processes own to the structure of the leaf and its pigment content. Hereby it is shown that red Chl fluorescence is highly determined by the absorption peak of chlorophyll around the 681 nm, while the bidirectional far-red Chl fluorescence is influenced by scattering properties of the leaf. Nevertheless, differences in relative share of upward or downward Chl fluorescence in the total amount (e.g., $\downarrow F/F_{\text{tot}}$) are quite small among species.

Also, it is shown that parameters characterizing the shape of the F spectrum (e.g., $\uparrow F_{681}/\uparrow F_{755}$ and $\downarrow F_{681}/\downarrow F_{755}$) are to an extent influenced by the within-leaf's light scattering properties, which effect will probably increase when Chl fluorescence is studied from the canopy scale. The considerable amount of far-red Chl fluorescence emitted downward should, moreover, be taken into account when interpreting the sun-induced Chl fluorescence signal at different scales, i.e. leaf, canopy, landscape. It is hypothesized that tall, heterogeneous canopies lead to an overall more hemispherically scattered SIF flux in the far-red and NIR, and therefore relatively lower at-sensor SIF intensity as opposed to more homogeneous and structurally simpler canopies.

Acknowledgments

The research presented in this paper is funded by the Belgian Science Policy Office (BELSPO) in the frame of the STEREO II program-project BIOHYPE (SR/00/131) and partially supported by the Spanish Ministry for Science and Innovation under the project AYA 2010-21432-C02-01. The authors wish to thank Adrian Del Amo for field assistance and laboratory analyses. We would also like to thank the anonymous reviewers for suggestions and improvements to the manuscript, and Luis Guanter for adding useful comments on the upscaling section.

References

- Agati, G. (1998). Response of the in vivo chlorophyll fluorescence spectrum to environmental factors and laser excitation wavelength. *Pure and Applied Optics*, 7, 797–807.
- Alonso, L., Gómez-Chova, L., Vila-Francés, J., Amorós-López, J., Guanter, L., Calpe, J., et al. (2007). Sensitivity analysis of the Fraunhofer Line Discrimination method for the measurement of chlorophyll fluorescence using a field spectroradiometer. *Proceedings of the 3rd International Workshop on Remote Sensing of Vegetation Fluorescence, Florence, Italy* (7–9 February).
- Amorós-López, J., Gómez-Chova, L., Vila-Francés, J., Alonso, L., Calpe, J., Moreno, J., et al. (2008). Evaluation of remote sensing of vegetation fluorescence by the analysis of diurnal cycles. *International Journal of Remote Sensing*, 29, 5423–5436.
- Buschmann, C. (2007). Variability and application of the chlorophyll fluorescence emission ratio red/far-red of leaves. *Photosynthesis Research*, 92, 261–271.
- Cade, B.S., & Noon, B.R. (2003). A gentle introduction to quantile regression for ecologists. *Frontiers in Ecology and the Environment*, 1, 412–420.
- Curran, P.J., Dungan, J.L., & Peterson, D.L. (2001). Estimating the foliar biochemical concentration of leaves with reflectance spectrometry testing the Kokaly and Clark methodologies. *Remote Sensing of Environment*, 76, 349–359.
- D'Ambrosio, N., Szabo, K., & Lichtenhaller, H.K. (1992). Increase of the chlorophyll fluorescence ratio F_{690}/F_{735} during the autumnal chlorophyll breakdown. *Radiation and Environmental Biophysics*, 31, 51–62.
- Damm, A., Guanter, L., Laurent, V.C.E., Schaeppman, M.E., Schickling, U., & Rascher, U. (2014). FLD-based retrieval of sun-induced chlorophyll fluorescence from medium spectral resolution airborne spectroscopy data. *Remote Sensing of Environment*, 256–266.
- Daumard, F., Goulas, Y., Champagne, S., Fournier, A., Ounis, A., Olioso, A., et al. (2012). Continuous monitoring of canopy level sun-induced chlorophyll fluorescence during the growth of a sorghum field. *IEEE Transactions on Geoscience and Remote Sensing*, 50, 4292–4300.
- Delegido, J., Van Wittenberghe, S., Ortiz, V., Verrelst, J., Veroustraete, F., Valcke, R., et al. (2014). Chlorophyll content mapping of urban vegetation in the City of Valencia based on the hyperspectral NAOC index. *Ecological Indicators*, 40, 34–42.
- Flexas, J., Escalona, J.M., Evain, S., Gulias, J., Moya, I., Osmond, C.B., et al. (2002). Steady-state chlorophyll fluorescence (F_s) measurements as a tool to follow variations of net CO_2 assimilation and stomatal conductance during water-stress in C3 plants. *Physiologia Plantarum*, 114, 231–240.
- Fournier, A., Daumard, F., Champagne, S., Ounis, A., Goulas, Y., & Moya, I. (2012). Effect of canopy structure on sun-induced chlorophyll fluorescence. *ISPRS Journal of Photogrammetry and Remote Sensing*, 68, 112–120.
- Frankenberg, C., Fisher, J.B., Worden, J., Badgley, G., Saatchi, S.S., Lee, J.E., et al. (2011). New global observations of the terrestrial carbon cycle from GOSAT: Patterns of plant fluorescence with gross primary productivity. *Geophysical Research Letters*, 38.
- Garrigues, S., Lacaze, R., Baret, F., Morissette, J.T., Weiss, M., Nickeson, J.E., et al. (2008). Validation and intercomparison of global Leaf Area Index products derived from remote sensing data. *Journal of Geophysical Research – Biogeosciences*, 113, <http://dx.doi.org/10.1029/2003GB002199>.
- Gitelson, A.A., Buschmann, C., & Lichtenhaller, H.K. (1998). Leaf chlorophyll fluorescence corrected for re-absorption by means of absorption and reflectance measurements. *Journal of Plant Physiology*, 152, 283–296.
- Guanter, L., Alonso, L., Gómez-Chova, L., Meroni, M., Preusker, R., Fischer, J., et al. (2010). Developments for vegetation fluorescence retrieval from spaceborne high-resolution spectrometry in the O(2)-A and O(2)-B absorption bands. *Journal of Geophysical Research – Atmospheres*, 115.
- Guanter, L., Frankenberg, C., Dudhia, A., Lewis, P.E., Gomez-Dans, J., Kuze, A., et al. (2012). Retrieval and global assessment of terrestrial chlorophyll fluorescence from GOSAT space measurements. *Remote Sensing of Environment*, 121, 236–251.
- Guanter, L., Zhang, Y.G., Jung, M., Joiner, J., Voigt, M., Berry, J.A., et al. (2014). Global and time-resolved monitoring of crop photosynthesis with chlorophyll fluorescence. *Proceedings of the National Academy of Sciences of the United States of America*, 111, E1327–E1333.
- Joiner, J., Guanter, L., Lindstrom, R., Voigt, M., Vasilkov, A.P., Middleton, E.M., et al. (2013). Global monitoring of terrestrial chlorophyll fluorescence from moderate-spectral-resolution near-infrared satellite measurements: Methodology, simulations, and application to GOME-2. *Atmospheric Measurement Techniques*, 6, 2803–2823.
- Joiner, J., Yoshida, Y., Vasilkov, A.P., Yoshida, Y., Corp, L.A., & Middleton, E.M. (2011). First observations of global and seasonal terrestrial chlorophyll fluorescence from space. *Biogeosciences*, 8, 637–651.
- Knyazikhin, Y., Schull, M., Stenberg, P., Mattus, M., Rautiainen, M., Yang, Y., et al. (2013). Hyperspectral remote sensing of foliar nitrogen content. *Proceedings of the National Academy of Sciences of the United States of America*, 110(3), 811–812 (E185–E192).
- Koenker, R., & Bassett, G. (1978). Regression quantiles. *Econometrica*, 46, 33–50.
- Koenker, R., & Hallock, K.F. (2001). Quantile regression. *Journal of Economic Perspectives*, 15, 143–156.
- Kraft, S., Bézy, J.-L., Del Bello, U., Berlich, R., Drusch, M., Franco, R., et al. (2013). FLORIS: Phase a status of the fluorescence imaging spectrometer of the earth explorer mission candidate FLEX. *Proceedings of SPIE The International Society for Optical Engineering*, 8889.
- Krause, G.H., & Weis, E. (1991). Chlorophyll fluorescence and photosynthesis – The basics. *Annual Review of Plant Physiology and Plant Molecular Biology*, 42, 313–349.
- Lichtenhaller, H. K., & Buschmann, C. (2001). Extraction of photosynthetic tissues: Chlorophylls and carotenoids. In R. E. Wrolstad, T. E. Acree, E. A. Decker, M. H. Penner, D. S. Reid, & S. J. Schwartz (Eds.), *Current protocols in food analytical chemistry* (pp. F4.2.1–F4.2.6). New York: John Wiley and Sons.
- Louis, J., Cerovic, Z.G., & Moya, I. (2006). Quantitative study of fluorescence excitation and emission spectra of bean leaves. *Journal of Photochemistry and Photobiology B – Biology*, 85, 65–71.

- Meroni, M., Busetto, L., Colombo, R., Guanter, L., Moreno, J., & Verhoef, W. (2010). Performance of spectral fitting methods for vegetation fluorescence quantification. *Remote Sensing of Environment*, 114, 363–374.
- Meroni, M., Rossini, M., Guanter, L., Alonso, L., Rascher, U., Colombo, R., et al. (2009). Remote sensing of solar-induced chlorophyll fluorescence: Review of methods and applications. *Remote Sensing of Environment*, 113, 2037–2051.
- Miller, J. R., Berger, M., Goulas, Y., Jacquemoud, S., Louis, J., Mohammed, G., et al. (2005). Development of a vegetation fluorescence canopy model – Final report.
- Moreno, J. F., Asner, G. P., Belenguer, T., Bell, A., Buschmann, C., Calera, A., et al. (2006). Fluorescence explorer (FLEX): An optimised payload to map vegetation photosynthesis from space. *AIAA 57th International Astronautical Congress*, 3. (pp. 2065–2074).
- Morissette, J.T., Baret, F., Privette, J.L., Myneni, R.B., Nickeson, J.E., Garrigues, S., et al. (2006). Validation of global moderate-resolution LAI products: A framework proposed within the CEOS Land Product Validation subgroup. *IEEE Transactions on Geoscience and Remote Sensing*, 44, 1804–1817.
- Moya, I., Daumard, F., Moise, N., Ounis, A., & Goulas, Y. (2006). First airborne multiwavelength passive chlorophyll fluorescence measurements over La Mancha (Spain) fields. *2nd International symposium on recent advances in quantitative remote sensing*. (pp. 820–825).
- Papageorgiou, G. C., & Govindjee (2004). *Chlorophyll a fluorescence – A signature of photosynthesis*. Springer, 818.
- Pedrós, R., Goulas, Y., Jacquemoud, S., Louis, J., & Moya, I. (2010). FluorMODleaf: A new leaf fluorescence emission model based on the PROSPECT model. *Remote Sensing of Environment*, 114, 155–167.
- Perez-Priego, O., Zarco-Tejada, P.J., Miller, J.R., Sepulcre-Canto, G., & Fereres, E. (2005). Detection of water stress in orchard trees with a high-resolution spectrometer through chlorophyll fluorescence in-filling of the O-2-A band. *IEEE Transactions on Geoscience and Remote Sensing*, 43, 2860–2869.
- Porcar-Castell, A., Tyystjärvi, E., Atherton, J., Van der Tol, C., Flexas, J., Pfundel, E. E., et al. (2014). Linking chlorophyll a fluorescence to photosynthesis for remote sensing applications: Mechanisms and challenges. *Journal of Experimental Botany*, 65(15), 4065–4095.
- Rautiainen, M., Heiskanen, J., Eklundh, L., Mottus, M., Lukes, P., & Stenberg, P. (2010). Ecological applications of physically based remote sensing methods. *Scandinavian Journal of Forest Research*, 25, 325–339.
- Rautiainen, M., & Stenberg, P. (2005). Application of photon recollision probability in coniferous canopy reflectance simulations. *Remote Sensing of Environment*, 96, 98–107.
- Thenkabail, P.S., Enclona, E.A., Ashton, M.S., & Van der Meer, B. (2004). Accuracy assessments of hyperspectral waveband performance for vegetation analysis applications. *Remote Sensing of Environment*, 91, 354–376.
- Van Wittenbergh, S., Alonso, L., Verrelst, J., Hermans, I., Delegido, J., Veroustraete, F., et al. (2013). Upward and downward solar-induced chlorophyll fluorescence yield indices of four tree species as indicators of traffic pollution in Valencia. *Environmental Pollution*, 173, 29–37.
- Van Wittenbergh, S., Alonso, L., Verrelst, J., Hermans, I., Valcke, R., Veroustraete, F., et al. (2014). A field study on solar-induced chlorophyll fluorescence and pigment parameters along a vertical canopy gradient of four tree species in an urban environment. *Science of the Total Environment*, 466–467, 185–194.
- Van Wittenbergh, S., Verrelst, J., Rivera, J.P., Alonso, L., Moreno, J., & Samson, R. (2014). Gaussian processes retrieval of leaf parameters from a multi-species reflectance, absorbance and fluorescence dataset. *Journal of Photochemistry and Photobiology B – Biology*, 134, 37–48.
- Verrelst, J., Alonso, L., Camps-Valls, G., Delegido, J., & Moreno, J. (2012). Retrieval of vegetation biophysical parameters using Gaussian process techniques. *IEEE Transactions on Geoscience and Remote Sensing*, 50, 1832–1843.
- Verrelst, J., Alonso, L., Rivera, J.P., Moreno, J., & Camps-Valls, G. (2013). Gaussian process retrieval of chlorophyll content from imaging spectroscopy data. *IEEE Journal of Selected Topics in Applied Earth Observations and Remote Sensing*, 6(2), 867–874.
- Vogelmann, T.C., & Han, T. (2000). Measurement of gradients of absorbed light in spinach leaves from chlorophyll fluorescence profiles. *Plant, Cell and Environment*, 23, 1303–1311.
- Zarco-Tejada, P.J., Gonzalez-Dugo, V., & Berni, J.A.J. (2012). Fluorescence, temperature and narrow-band indices acquired from a UAV platform for water stress detection using a micro-hyperspectral imager and a thermal camera. *Remote Sensing of Environment*, 117, 322–337.